This is an open access article published under an ACS AuthorChoice License, which permits copying and redistribution of the article or any adaptations for non-commercial purposes.

ACS APPLIED BIO MATERIALS

www.acsabm.org Article

Physical Confinement Impacts Cellular Phenotypes within Living Materials

Hans Priks,[§] Tobias Butelmann,[§] Aleksandr Illarionov, Trevor G. Johnston, Christopher Fellin, Tarmo Tamm, Alshakim Nelson, Rahul Kumar,* and Petri-Jaan Lahtvee*

Cite This: *ACS Appl. Bio Mater.* 2020, 3, 4273–4281 Read Online

ACCESS | Metrics & More | Article Recommendations | Supporting Information

ABSTRACT: Additive manufacturing allows three-dimensional printing of polymeric materials together with cells, creating living materials for applications in biomedical research and biotechnology. However, an understanding of the cellular phenotype within living materials is lacking, which is a key limitation for their wider application. Herein, we present an approach to characterize the cellular phenotype within living materials. We immobilized the budding yeast *Saccharomyces cerevisiae* in three different photo-cross-linkable triblock polymeric hydrogels containing F127-bis-urethane methacrylate, F127-dimethacrylate, or poly(alkyl glycidyl ether)-dimethacrylate. Using optical and scanning electron microscopy, we showed that hydrogels based on these polymers were stable under physiological conditions, but yeast colonies showed differences in the interaction within the living materials. We found that the physical confinement, imparted by compositional and structural properties of the hydrogels, impacted the cellular phenotype by reducing the size of cells in living materials compared with suspension cells. These properties also contributed to the differences in immobilization patterns, growth of colonies, and colony coatings. We observed that a composition-dependent degradation of polymers was likely possible by cells residing in the living materials. In conclusion, our investigation highlights the need for a holistic understanding of the cellular response within hydrogels to facilitate the synthesis of application-specific polymers and the design of advanced living materials in the future.

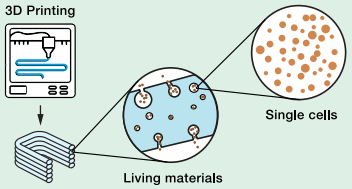

KEYWORDS: *living materials, triblock copolymers, hydrogels, additive manufacturing, 3D printing, yeast, cell size, polymer degradation, scanning electron microscopy, bioprocessing, biotechnology*

INTRODUCTION

Three-dimensional (3D) printing of natural and synthetic materials for biomedical and biotechnology applications is a promising research field with applications that include screening tools and production platforms in a sustainable economy.[1] Self-assembling block copolymer hydrogels have been demonstrated for extrusion-based 3D printing and offer exciting opportunities to create synthetic polymer hydrogel networks that can immobilize microbial cells and recapitulate the environment of a biofilm.[2,3] These microbe-laden hydrogels form living materials (LMs) that are permissive for metabolic activity and can provide significant improvement with respect to robustness, reproducibility, and scale-up over traditional immobilization methods using natural biopolymers.[4] The multiscale properties of hydrogels of such polymers allow their applications in diverse fields, such as drug delivery,[5] tissue engineering,[6] and biotechnology.[4,7] Precise material deposition, together with a high degree of spatial control, allows the manufacturing of predesigned and custom-made structures.[8,9] One prominent triblock copolymer hydrogel for extrusion-based printing is based on Pluronic F127, which embodies dual-responsive properties toward temperature (sol at 4 °C, gel at 25 °C) and the applied shear forces.[10] This ABA triblock copolymer, wherein the "A" blocks are hydrophilic poly(ethylene oxide) (PEO) and the "B" block is a hydrophobic poly(propylene oxide), can self-assemble to form micelles in aqueous solution. As the concentration of F127 in solution increases, the polymer reaches a critical gel concentration. The Nelson group recently developed BAB triblock copolymer hydrogels for direct-write extrusion printing with hydrophobic poly(alkyl glycidyl ether) "B" blocks that flank a central poly(ethylene oxide) "A" block that exhibits similar stimuli-responsive behaviors to F127.[11] In contrast to F127, the BAB triblock copolymers form reverse flower micelles in solution.[11−13] Furthermore, the chain-end modification of BAB and ABA triblock copolymers allows for cross-linking by means of photo-initiated polymerization while or after completion of the 3D printing process to afford robust hydrogel structures.[14−16] Polymer hydrogels based on F127-dimethacrylate (F127-DMA), F127-bisurethane methacrylate (F127-BUM), and poly(isopropyl glycidyl ether-*stat*-ethyl glycidyl ether)-*block*-poly(ethylene oxide)-*block*-poly(isopropyl glycidyl ether-*stat*-ethyl glycidyl ether) dimethacrylate (PGE-

Received: March 26, 2020
Accepted: June 7, 2020
Published: June 7, 2020

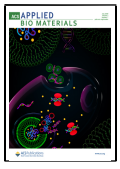

ACS Publications © 2020 American Chemical Society

https://dx.doi.org/10.1021/acsabm.0c00335
ACS Appl. Bio Mater. 2020, 3, 4273–4281

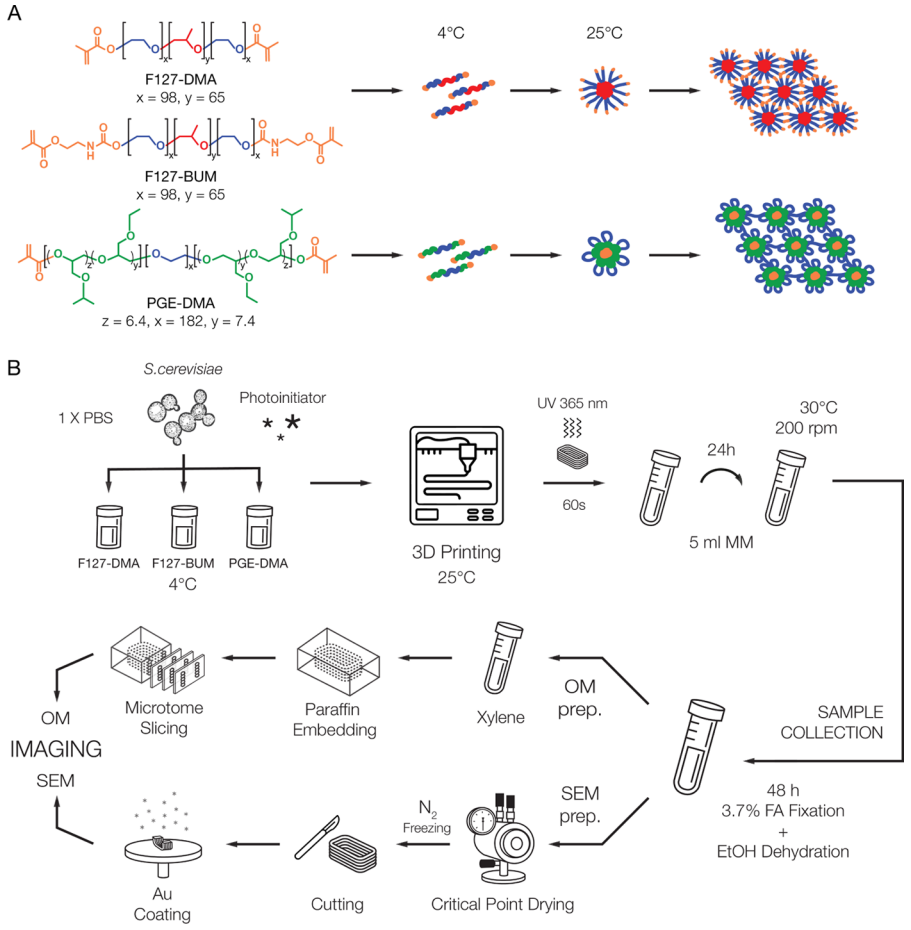

Figure 1. Schematic diagram showing polymer chemistry (A) and experiment workflow (B). The polymers were mixed with phosphate-buffered saline (PBS), cells, and photoinitiator at 4 °C and printed at 25 °C to be cured after printing. Batch cultivation time was 24 h for varying days. Samples were collected, fixed, and dehydrated. Specific preparation protocols were applied for SEM or OM imaging.

DMA) have previously been reported for encapsulation and direct-write extrusion printing of microbes.[4,17−19] In all of these cases, the hydrogels maintained the viability and metabolic activity of yeast or bacteria to afford immobilized bioreactors with long-term metabolic activity.[4,17,18]

Methods for the characterization of the physicochemical properties of such hydrogels, particularly their stiffness, swelling ratio, and rheology, are well established.[20,21] However, similar robust analysis methodologies for understanding cellular phenotypes of microbial cells confined within hydrogels are lacking but necessary, before LM-based technologies could be used in specific, reproducible, and efficient processes. Previously, optical microscopy (OM) and scanning electron microscopy (SEM) have been used to investigate cell-gel morphology[22−24] and hydrogels themselves[24−26] but only to an illustrative extent. For this reason, we focused on these reliable and accessible microscopy tools and techniques for the characterization of LMs and for the investigation of cellular phenotypes in a physiological environment. In all instances, we used the budding yeast *Saccharomyces cerevisiae*, which has been previously reported to be viable in these materials and assigned the generally recognized as safe (GRAS)[27] status making it applicable in food and pharma industries.[4,17,18] In our study, we selected three different functionalized triblock copolymers: F127-DMA,[4] F127-BUM,[17,19] and PGE-DMA.[18] These polymers are advantageous over calcium alginate for microbial encapsulation because the materials are covalently cross-linked and charge-neutral. The carboxylate groups of alginate have previously been shown to inhibit the transport of ions through these hydrogel matrices.[17] We investigated the stability and degradation of the hydrogels of these polymers after cultivation in a physiological environment, the polymer−cell interface, the localization of cells, the proliferation of colonies, the effect of cellular growth on the polymers, and the effect of physical confinement on the cellular phenotype using both OM and SEM methods. Further, we used a computational approach for SEM image analysis to determine cell size changes in living materials and suspension cell cultures. This allowed us to assess the effects of different polymers on the cellular phenotype, which is important for a holistic understanding of LMs and the selection for particular applications. The detailed workflow of our study is illustrated in Figure 1.

MATERIALS AND METHODS

Chemical Synthesis of Polymers. Two F127-derived polymers, namely, F127-BUM and F127-DMA, and PGE-DMA were provided by the Nelson laboratory at the University of Washington. The synthesis of these polymers has been fully described in the laboratory's previous publications.[4,18,19] The percent (%) functionalization for F127-DMA was 81%, while F127-BUM and PGE-DMA were functionalized quantitatively.

F127-DMA. The F127-DMA polymer used in this study was synthesized using methacryloyl chloride as described in the literature.[4] Briefly, Pluronic F127 was dried and subsequently dissolved in anhydrous toluene under a nitrogen atmosphere. Triethylamine was

https://dx.doi.org/10.1021/acsabm.0c00335
ACS Appl. Bio Mater. 2020, 3, 4273−4281

added, and the solution was cooled to 0 °C. A solution of methacryloyl chloride in anhydrous toluene was added dropwise to the solution. After complete addition of the methacryloyl chloride solution, the reaction mixture was warmed to room temperature and allowed to stir for 24 h. The polymer was collected *via* vacuum filtration, concentrated under reduced pressure, and reconstituted in fresh toluene. This process was repeated two more times. The polymer was once again dissolved in toluene and precipitated in diethyl ether. The polymer was rinsed twice with fresh ether and collected *via* centrifugation. The polymer was dried in a vacuum oven to afford a fluffy, white powder.

F127-BUM. The F127-BUM polymer used in this study was synthesized using 2-isocyanatoethyl methacrylate and dibutyltin dilaurate according to the literature.[19] Briefly, Pluronic F127 was dried and subsequently dissolved in anhydrous dichloromethane (DCM). Dibutyltin dilaurate was added to the mixture, followed by the dropwise addition of a 2-isocyanatoethyl methacrylate/DCM solution. The reaction was allowed to stir for 2 days, quenched with methanol, and precipitated in diethyl ether. The polymer was collected *via* centrifugation and washed twice with fresh ether. The polymer was dried under vacuum to afford a fluffy, white powder.

Unfunctionalized PGE. The unfunctionalized PGE precursor polymer was synthesized by anionic ring-opening polymerization as described in the literature.[11] Briefly, PEO was added to the reaction vessel and dried under vacuum overnight. Dry tetrahydrofuran (THF) was added and a potassium naphthalenide solution was titrated into the flask under an argon atmosphere. Isopropyl glycidyl ether and ethyl glycidyl ether were added simultaneously to begin polymerization. The reaction continued for 24 h at 65 °C. The reaction mixture was then precipitated into cold hexane and washed twice. The isolated polymer was dried in a vacuum oven to afford the unfunctionalized PGE polymer precursor as an off-white solid.

PGE Methacrylate. The methacrylate-functionalized PGE polymer used in this study was synthesized using methacrylic anhydride as described in the literature.[18] Briefly, the PGE polymer precursor was dissolved in dry THF under a nitrogen atmosphere. Triethylamine was added, and the mixture was heated at 65 °C for 30 min. Methacrylic anhydride was then added, and the mixture was stirred for 16 h at 65 °C. The reaction mixture was then precipitated into cold ether. The polymer was collected and washed twice with additional ether, once with hexane, and dried under vacuum for 24 h to afford the methacrylate-functionalized PGE polymer (PGE-DMA) as an off-white solid.

Yeast Strain, Media, and Cultivation Conditions. The yeast strain *S. cerevisiae* CEN.PK113-7D (*MATa*, *MAL2-8*^{c}, *SUC2*) was used throughout the study and cultivated in minimal medium (MM). The composition of 1 L of MM (pH = 6.9) was 10 g of glucose (Acros Organics), 2.5 g of $(NH_4)_2SO_4$ (Lach-Ner), 3 g of KH_2PO_4 (Sigma-Aldrich), 5.25 g of K_2HPO_4 (Merck), and 0.25 g of $MgSO_4$ (Sigma-Aldrich) in Milli-Q water. One milliliter of trace elements (all Sigma-Aldrich, unless marked differently) and 1 mL of vitamin solution (all Sigma-Aldrich, unless marked differently) were added after sterilization of the MM. One liter of trace element solution (pH = 4) contained ethylenediaminetetraacetic acid (EDTA) sodium salt (Lach-Ner), 15.0 g; $ZnSO_4{\cdot}7H_2O$, 4.5 g; $MnCl_2{\cdot}2H_2O$, 0.84 g; $CoCl_2{\cdot}6H_2O$, 0.3 g; $CuSO_4{\cdot}5H_2O$, 0.3 g; $Na_2MoO_4{\cdot}2H_2O$, 0.4 g; $CaCl_2{\cdot}2H_2O$ (Carl Roth), 4.5 g; $FeSO_4{\cdot}7H_2O$, 3.0 g; H_3BO_3, 1.0 g; and KI, 0.1 g. One liter of vitamin solution (pH = 6.5) contained biotin, 0.05 g; *p*-amino benzoic acid, 0.2 g; nicotinic acid, 1 g; Ca pantothenate, 1 g; pyridoxine-HCl, 1 g; thiamine−HCl, 1 g; and myoinositol (AppliChem), 25 g; in Milli-Q water. Where indicated, a SIGMAFAST inhibitor cocktail (S8820, Sigma-Aldrich) was used in MM at a concentration of 0.1x according to the manufacturer. Cell cultivation was carried out in 15 mL tubes (5 mL MM) at 30 °C and 200 rpm in an incubator. The living materials were washed in 70% ethanol (Berner Pro) for 60 s after printing and equilibration to avoid contamination and viable yeast on the surface of living materials. A short wash in 70% ethanol was applied after every 24 h batch.

Hydrogel Preparation for 3D Printing. Sterile phosphate-buffered saline (PBS) solution was mixed with a desired polymer and cooled at 4 °C overnight to prepare a hydrogel (F127 hydrogels: 30 wt %, PGE-DMA: 20 wt %). One liter of PBS (pH = 7.2) contained 8 g of NaCl (Sigma-Aldrich), 1.44 g of Na_2HPO_4 (Fisher Scientific), 0.24 g of KH_2PO_4, and 0.2 g of KCl in Milli-Q water. To make a hydrogel ready for printing, 1.5 μL g^{-1} hydrogel of the photoinitiator 2-hydroxy-2-methylpropiophenone (Irgacure 1173; >97%, Sigma-Aldrich) was added at a temperature of 4 °C. If needed, 10^5 or 10^6 spun-down cells g^{-1} hydrogel were added. A short stirring of both additives ensured an equal distribution, and after incubating for 30 min on ice, to make the solution bubble-free, it was poured into a 10 mL dispensing barrel equipped with a 0.41 mm dispensing tip (both Adhesive Dispensing, United Kingdom) and warmed to room temperature to transform into a shear-responsive state for printing.

3D Printing. Three-dimensional printing was performed on a K8200 printer (Velleman, Belgium) modified to be applicable for direct pressure dispensation. The computer-aided design model was designed with Solidworks (Student Edition), and the G-code was generated using open source 3D printing toolbox (Slic3r 1.3.0). The model's measures were 10 mm × 3 mm × 3.5 mm (*X*, *Y*, *Z*) sliced with one outer perimeter and printed in vase mode with a print speed of 10 mm s^{-1}. Directly after the print, the hydrogel was cross-linked for 60 s with four light-emitting diodes (CUN66A1B, Seoul Viosys, Republic of Korea) emitting at a wavelength of 365−367 nm.

High-Performance Liquid Chromatography. Chromatography was performed using an Aminex HPX-87H Column (Bio-Rad) with 5 mM sulfuric acid (>99.5%, Merck) as a mobile phase at 45 °C. A Shimadzu Prominence-i LC-2030C Plus (Japan) equipped with a Refractive Index Detector RID-20A (Shimadzu, Japan) was used to detect the components.

Fourier Transform Infrared (FTIR) Spectroscopy. FTIR spectroscopy was used to obtain structural information about the polymers. Polymers were dried for 24 h at 25 °C in 1 mbar vacuum (VO200, Memmert, Germany). The measurements were performed using an Alpha spectrometer equipped with Platinum ATR (Bruker). The polymers were analyzed over the range of 3800−400 cm^{-1} and averaging was over 24 spectra each.

Macroscopic Observations. Samples were arranged and imaged on a Petri dish after the indicated amount of time. Pictures were acquired with a Canon EOS 450D equipped with a Canon Zoom Lens EF 17−40 mm.

Scanning Electron Microscopy. *Sample Fixation and Dehydration.* The samples were fixed for 48 h in 3.7% formaldehyde (Biotop/Naxo) in 0.1 M phosphate buffer (PB) fixation solution, which was replaced after 24 h. One liter of 0.2 M phosphate buffer contained 20.44 g of Na_2HPO_4 and 6.72 g of NaH_2PO_4 (Acros Organics). For sample dehydration, 99.5% ethanol was used to establish several dilutions of it in Milli-Q water. Samples were dehydrated in an ascending ethanol series (40−90%, 10% steps; 96%, 99.5%) at room temperature (2 h minimum per step; last step overnight followed by replacement with fresh absolute ethanol).

Critical Point Drying. A critical point dryer (E3100, Quorum Technologies, United Kingdom) was cooled to 15 °C with a thermostat (Proline RP 1845, LAUDA, Germany). The samples were mounted on a tray and inserted into the critical point dryer. The dryer was filled with liquid CO_2 to replace the ethanol, and the chamber was purged 6−8 times in 30−60 min intervals. The critical point was reached by increasing the temperature to 37 °C and controlling the pressure not to exceed 110 bar, followed by pressure release to recover the samples. The pressure release was done either fast or slow. With slow release, pressure was released slowly overnight until the chamber was ready to be opened. With fast release, pressure from 110 to 60 bar was released slowly (to avoid cooling the reactor and turning the supercritical state back to the liquid state), and from there, the remaining pressure was released within 3 min. The samples shrank by 35−40% due to the drying process.

Sample Cutting. The samples were frozen in liquid N_2 and cut with a scalpel. For acquiring artifact-free cross sections, the sample and scalpel were immersed in liquid N_2 for 20 s and instantly cut with fast incisions. For acquiring information of colony−material interactions, colony size, and shape, the sample and scalpel were

https://dx.doi.org/10.1021/acsabm.0c00335
ACS Appl. Bio Mater. 2020, 3, 4273−4281

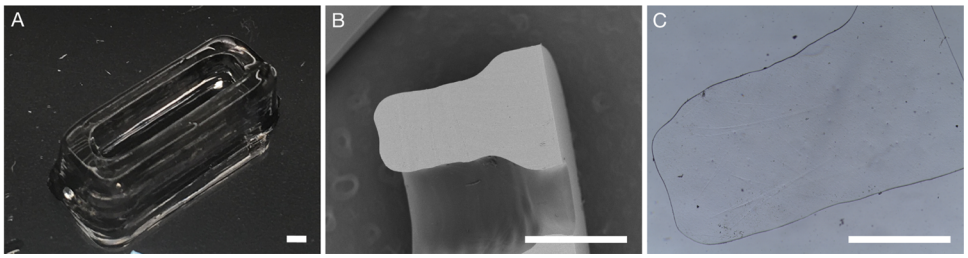

Figure 2. Illustrative images of control structures (hydrogels printed without cells). Photograph after 24 h equilibration (A). Cross-sectional SEM micrograph (B). OM micrograph; slice thickness 40 μm (C). Scale bar is 1 mm.

immersed in liquid N_2 for 10 s and then cut after 2−3 s at room temperature with slow incision.

Sputter Coating. A sample stub was covered with sticky carbon tape, and the cut sample was attached on it. The sample was coated with a 7.5 nm thick gold layer using a high vacuum sputter coater (EM ACE600, Leica Microsystems, Germany).

Imaging. Gold-coated samples were imaged with a tabletop scanning electron microscope (TM-3000, Hitachi, Japan), with a back-scattered electron detector. The imaging was done under a high vacuum and 15 kV accelerating voltage. Results were confirmed by imaging several samples over multiple slices. Colony sizes were directly detected using the measurement tool of the imaging software.

Image Analysis. SEM image analysis was performed using GIMP and MATLAB2019b with image processing toolbox. In this analysis, for cell size (volume in μm^3) calculations, yeast cells were assumed to have an ellipsoid shape. Cells were manually selected from electron microscopy images using GIMP. The resulting segmentation masks were then imported into MATLAB. Major (length) and minor (width) axes were calculated, and the length of the axis in the third dimension (height) was assumed to be equal to the length of the minor axis. Cell volume was then estimated using the formula for volume of an ellipsoid body.

Optical Microscopy. *Sample Preparation.* The sample fixation was carried out in the same way as mentioned for SEM and finally transferred to histo-grade xylene (J.T. Baker) for 1 h. The samples were then placed into paraffin-embedding cassettes and covered with liquid paraffin (Leica) at 65 °C for 1 h to ensure proper infusion. The sample was taken out, orientated on a metal tray and covered with liquid paraffin. The sample was then cooled down.

Sectioning and Rehydration. For microtome sections, a paraplast-embedded sample was mounted onto a microtome (RM2255, Leica Microsystems, Germany) and several slices were cut. The slice thickness was 40 μm. The slices were collected from a water bath (Milli-Q water) on a glass slide. The samples were dried overnight and then sequentially rehydrated in histo-grade xylene (20 min), 99.5% ethanol (20 min), 90% ethanol (20 min), and finally dH_2O (20 min).

Imaging. The rehydrated slices were carefully mounted on microscope glass slides and covered with ca. 40 μL of Milli-Q water and a cover glass. A DM750 microscope equipped with an ICC50 HD camera system (both Leica Microsystems, Germany) was used. Results were confirmed by imaging several slices.

RESULTS AND DISCUSSION

Stability of Cell-Free Hydrogels under Physiological Conditions. F127-DMA and F127-BUM hydrogels were prepared as 30 wt % in PBS buffer, while PGE-DMA was prepared as 20 wt %, and all formulations included 0.15 wt % 2-hydroxy-2-methylpropiophenone as a photoinitiator. These hydrogels have previously been shown to be printable using a direct-write extrusion printer.[4,17,18] Despite the fact that F127-DMA and F127-BUM were present at the same concentration in their respective hydrogels, the latter polymer resulted in hydrogels that had a larger storage modulus (247 vs 203 kPa).[4,19] The data were acquired in Milli-Q water, but the storage modulus pattern should remain relatively similar in PBS.[28] The difference in stiffness of F127-based gels is attributed to the presence of carbamate linkage at the polymer chain ends in F127-BUM (Figure S1), which can form intermolecular hydrogen bonds. The PGE-DMA hydrogel had a lower storage modulus (96 kPa) largely due to the lower concentration of the polymer present.[18] Concentrations of PGE-DMA beyond 20 wt % were not possible as the hydrogel became too stiff for processing. The lower feasible concentration for PGE-DMA gel formation is attributed to the difference in the self-assembled networks. In particular, the presence of bridging chains in BAB triblock copolymer assemblies could facilitate the gelation (Figure 1A).

We first sought to understand how cells proliferate and affect the surrounding hydrogel matrix, which was observed using OM and SEM. The stability of the cross-linked hydrogels in the absence of any cells was observed for 14 days in MM. The images presented here serve as a control (Figure 2) to appreciate the differences with yeast-laden hydrogels, where the structures might transform due to proliferation of cells. At both macroscopic and microscopic levels, the control samples appeared stable throughout the cultivation period under physiological conditions and no creep could be observed in any sample. Moreover, we also did not observe any changes in the physiological environment as determined by glucose and pH measurements (Figure S2A,B). The mass of the control structures remained unchanged.

Stability of Yeast-Laden Hydrogels. After ascertaining the stability of all hydrogels printed without cells, we focused on understanding the impact of long-term proliferation of immobilized cells on the hydrogels and whether different proliferation patterns were adopted by cells in the distinct LMs. Here, we printed the same formulations as mentioned before with a cell inoculum of 10^6 cells g^{-1} hydrogel using a direct-write extrusion printer. After ultraviolet curing, we washed each LM for 60 s in 70% ethanol to ensure sterility of printed structures and to avoid potential contamination of the culture medium from peripheral cells. We cultivated the LMs in 5 mL of MM for 14 days in at least triplicate with a change of medium every 24 h. Representative samples were collected for processing for either OM or SEM on days 0, 7, and 14. During sample fixation and dehydration for microscopy analysis, some cells detached from the cross-sectional surface.

Starting on day 0 (after equilibration for 24 h at room temperature), small colonies were observed inside the 3D-printed structures (Figure S4A,C,E,G,I,K). After 1 week, clear differences were observed in how cells grew inside each of the hydrogels; those distinct proliferation patterns remained largely consistent during the second week. Peripheral colonies in F127-based LMs tended to merge and formulate a separate film around LMs (Figure 3A,B,D,E). These materials cracked

https://dx.doi.org/10.1021/acsabm.0c00335
ACS Appl. Bio Mater. 2020, 3, 4273−4281

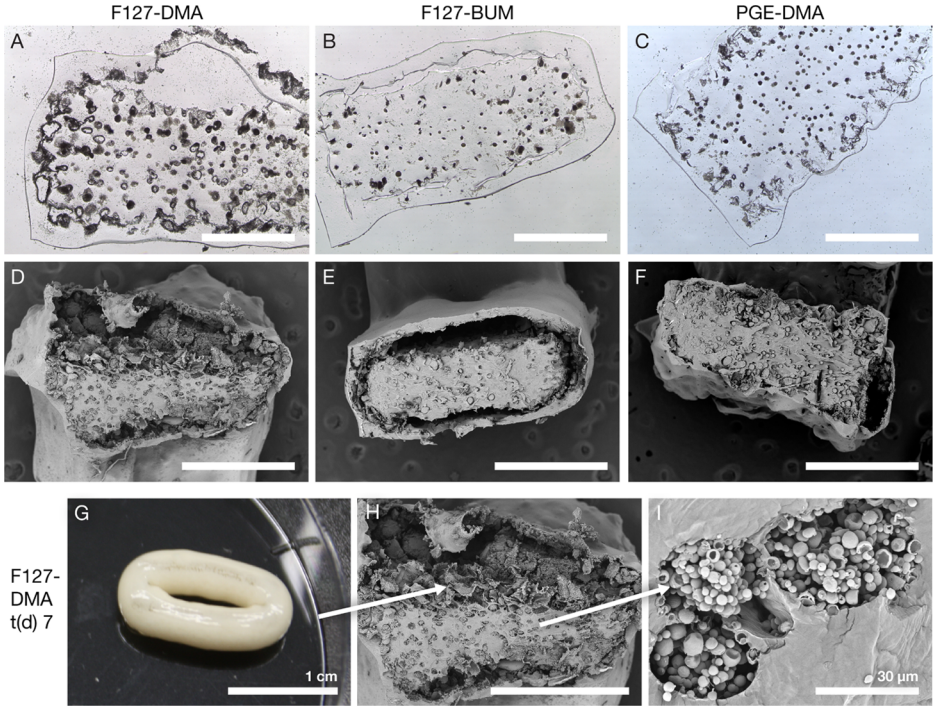

Figure 3. OM (A–C) and SEM (D–F, H, I) micrographs of LMs after 7 days of incubation. Cells escaped from PGE-DMA, without major disruption of the material, F127-DMA, and F127-BUM formed separated layers (center vs shell). Most cell proliferation occurred at the interface. The LMs swelled up and retained cells up to a particular cell number (G). As peripheral colonies joined into one major colony (G, H), the colonies residing in the middle of the hydrogel were deprived of access to nutrients causing cell death in colonies (I). Scale bar is 1 mm unless marked differently.

open beyond a particular cell number (Figure S4D,J). For some samples in F127-DMA, the cell-free layer and cell-laden layer tended to separate completely (Figures S4B,H and S5). The growth of colonies in PGE-DMA was directed toward the periphery (Figures 3C,F and S4F). A separated layer as in F127-based LMs was not observed. We observed that there was a colony diameter size gradient in all LMs, with smaller colonies in the middle and larger ones toward the periphery (Figure S6). Colony diameters in the middle of the structure for all three hydrogel compositions stayed in the range of 26–38 μm, with similar observations for day 7 and 14 samples (Figures 3 and S4). Cell-retaining structures became swollen due to cellular proliferation (Figure 3G), and colonies in the middle region started to show an altered morphology, indicating phenotypic differences in cells (Figure 3I). Potentially, there was a limitation of nutrients for inner cells that contributed toward a clear colony size gradient (Figure S6); the cells in the smaller, nutrient-limited inner colonies were also likely more prone to cell death (Figures 3I and S6). A similar pattern has been reported in a recent study by Qian and colleagues.[7] Here, the printing of thicker structures will not necessarily lead to more fermentation by cells, as they appear to be limited by nutrient diffusion to and from the central parts of the material.

Two days after the start of the experiment, glucose was always depleted within every 24 h batch cultivation (Figure S2C), and the pH did not drop substantially (Figure S2D). The cells started to escape into the culture medium at different time points. F127-DMA retained cells the longest (5.13 ± 1.55 days), whereas F127-BUM, although structurally almost identical, retained them for 3 days and PGE-DMA for 2 days (Figure S2E). F127-BUM did not perform as expected considering its storage modulus, so we assumed that another factor besides physical parameters might play a role in its performance, which is addressed in the polymer integrity analysis section. Due to growth, swelling, and retention time differences in F127-DMA and F127-BUM, the living materials were 136.80 (±27.78)% and 53.39 (±4.15)% heavier, respectively, after 1 week (Figure S2F). The observed mass increase was only 41.28 (±9.93)% for PGE-DMA (Figure S2F). After the cells started escaping from hydrogels, they were continuously washed out from the cavity between the inner and outer layers of F127-based materials and resulted in an increase of about 40% (relative to the start) after 2 weeks of cultivation (Figure S2F). However, since PGE-DMA did not form such cavities, its weight stayed the same during the second week (Figure S2F). Interestingly, the increase in mass was the same (roughly 40%) for all LMs after 2 weeks of incubation. This appears to be the carrying capacity of all tested living materials under our experimental conditions after 2 weeks and suggests that modifications to hydrogels would be necessary to increase the capacity in the future.

Growth Patterns of Yeast Colonies in Living Materials. To understand cellular growth within the hydrogels, we 3D-printed these materials with a lower number of cells (~10^5 g^{-1} hydrogel), allowing us to observe single colonies after 48 h of cultivation. Batch cultivation in 5 mL of MM was carried out with a medium change every 24 h. As observed before, cells were retained in both F127-DMA and F127-BUM hydrogels on day 2, whereas cells started to escape from PGE-DMA (Figure S7A). Therefore, the comparison of glucose consumption in PGE-DMA hydrogels with that in F127-based hydrogels was not possible from the second day onwards. Within 24 h, glucose was consumed slightly faster in

https://dx.doi.org/10.1021/acsabm.0c00335
ACS Appl. Bio Mater. 2020, 3, 4273–4281

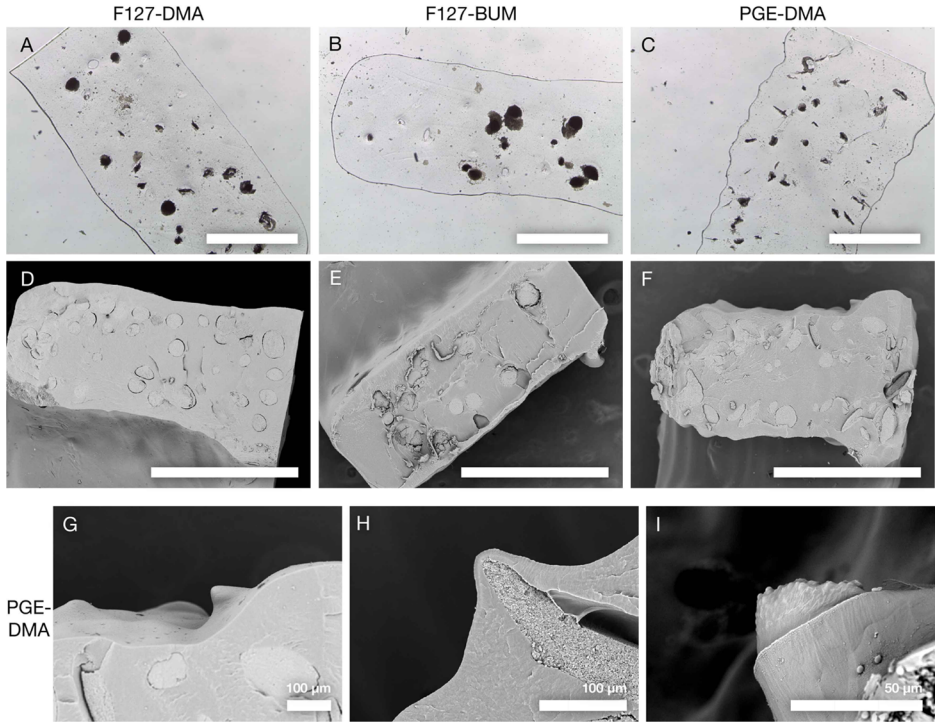

Figure 4. SEM and OM micrographs of LMs after 48 h of incubation (A–F) and the escape mode of cells from PGE-DMA (G–I). Peripheral colonies in PGE-DMA formed spindlelike structures (C, F, H), while F127-DMA and F127-BUM formed spherical colonies (A, B, D, E). When the material broke, cells started escaping into the medium (I). Scale bar is 1 mm unless marked differently.

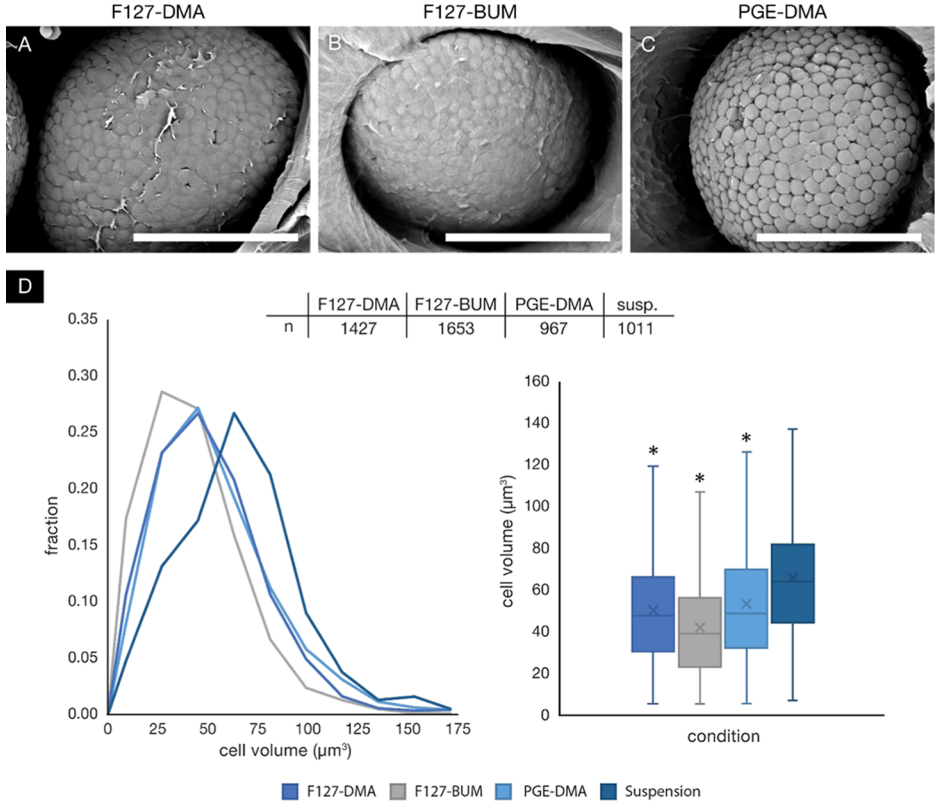

Figure 5. Organic film covers yeast cell colonies in LMs and cell volume (μm^3). F127-DMA (A) and F127-BUM (B) both had a thin organic coating around colonies, while PGE-DMA (C) lacked a similar polymer coating. Scale bar is 30 μm. Cell volume (in μm^3) distribution in LMs and suspension cell culture (D). A total of ≥967 cells per condition were analyzed. LMs were incubated for 48 h before processing and the measurement. *$p < 0.05$, significant difference from suspension cells, x: mean.

https://dx.doi.org/10.1021/acsabm.0c00335
ACS Appl. Bio Mater. 2020, 3, 4273–4281

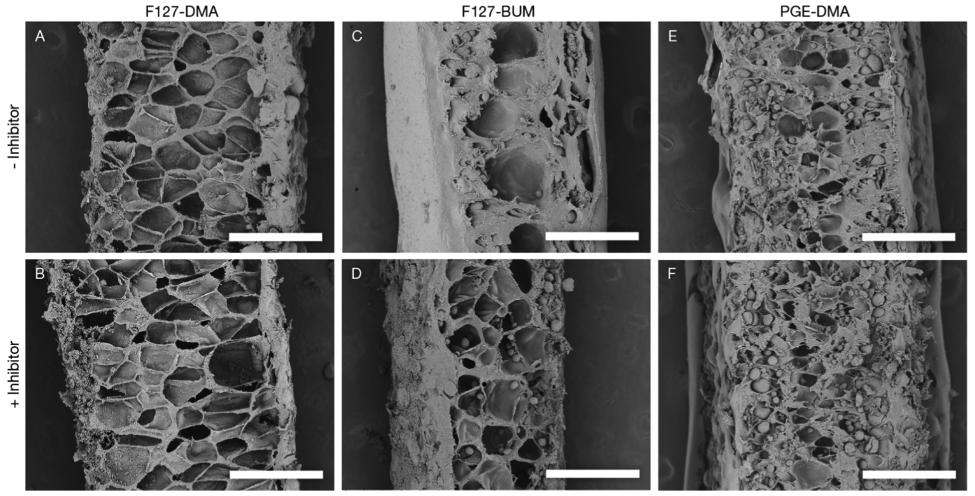

Figure 6. SEM micrographs showing cavities after pressure release of CO_2 inside LMs. Upper panel: normal cultivation; lower panel: enzyme inhibitors added into the MM. No visual differences were detected in DMA-functionalized polymers (A, B, E, F). Differences were observed in F127-BUM (C, D): when the enzyme inhibitors were missing, the material was degraded allowing the gas to escape more easily during sample preparation (C), whereas gas got trapped in intact material and formed more cavities (D). The experiment was conducted with 5 mL batches for 24 h over 14 days. All samples were prepared in a single supercritical CO_2 extraction process to avoid technical variations. Scale bar is 500 μm.

PGE-DMA and F127-DMA hydrogels compared to F127-BUM hydrogels, where the difference in starting/finishing glucose was only minimal (Figure S7B). After 48 h, glucose was consumed significantly more in the medium of F127-DMA than in F127-BUM, supporting the aforementioned observation (Figure S7B). The ABA block architecture of F127-DMA and F127-BUM as well as the BAB block architecture of PGE-DMA afford different physically and chemically cross-linked networks and storage moduli. Those differences, among others, further support differences in glucose diffusion through the hydrogel (Figure S7B). Further studies are required to assess the diffusion of molecules through these hydrogel matrices, wherein the polymer composition, architecture, and concentration are altered to design or select other LMs based on these diffusion parameters.[29,30]

Interestingly, the morphology of colonies differed between F127-based LMs and PGE-DMA hydrogels. While the colonies in F127-based materials were spherical in shape (Figure 4A,B,D,E), PGE-embedded colonies showed a more irregular spindlelike or elliptic shape (Figure 4C,F,H). For this reason, it was impossible to properly measure and compare the colony size and growth rate inside PGE-DMA relative to the F127-based hydrogels. Additionally, lesions appeared on the surface of PGE-DMA hydrogels, confirming the escape of cells into the medium (Figure 4I), which were not observed in F127-based hydrogels. After 72 h, the F127-based hydrogels had single colonies in the range of 90−250 μm, and the proliferation of the colonies toward the center of the hydrogel did not exhibit a significant change in size to the ones after 48 h (Figure S8). Taken together, the different growth patterns in F127-based materials and PGE-DMA were most likely driven by the micellar structure of the polymers.

Cellular Phenotyping in Living Materials. Further investigations of the cell-laden hydrogels revealed a thin organic coating around the cell colonies in the F127-DMA and F127-BUM hydrogels (Figure 5A,B), which was not present in the PGE-DMA hydrogels (Figure 5C). This difference became evident within 24 h after 3D printing and incubation at room temperature. A thin film was possibly formed due to a different micellar identity of these polymers allowing distinct interactions with cells (hydrophilic membranes) that likely resulted in a different alignment of micelles around cells before photo-cross-linking by UV. A supercritical CO_2 extraction protocol was used with a rapid release of CO_2 to separate and measure the thin polymer coating (100−160 nm) around yeast colonies (Figure S3.2D). As colonies increased in size, the thin surrounding coating ruptured, and only remnants of the coating were observed on a colony surface (Figure S9). Based on SEM images, we determined that the film ruptured when the colony diameter had reached a size of about 60−80 μm within the LMs (Figure S9).

The different cell−polymer interactions, as well as retention times, consequently led to the question of impact of physical confinement on the cell phenotype. To address this question, we performed a computational analysis on the acquired SEM images as described in the Materials and Methods section. During this analysis, the cell size (volume in μm^3) parameter was utilized to investigate the effects of physical confinement on the cells in hydrogels in comparison to suspension cells. We evaluated cell size differences after 48 h in the aforementioned samples (used in Figure 4). Suspension cells were cultivated, fixed, and dehydrated in the same way as the immobilized cells (Figure S10). Interestingly, cells encapsulated in hydrogels were significantly ($p < 0.05$) smaller than the suspension cells (Figure 5D). Cell size differences were even evident among the LMs (Figure 5D). The cause of cell size differences was likely multifarious instead of an individual attributable factor, as a cellular phenotype is an integrated readout of manifold cellular processes, and naturally, physical confinement in hydrogels is an additional factor for immobilized cells compared to suspension cells (Figure 5). Nevertheless, our data suggests that a higher storage modulus led to smaller cell size. Previous studies on effects of physical confinement in a calcium alginate matrix indicate changes in cellular physiology of yeast.[31,32] Although a molecular investigation of cells was not in the scope of the present study, it would be very valuable to understand underlying molecular mechanisms responsible for phenotypic differences in LMs for their development as a technology of the future.

https://dx.doi.org/10.1021/acsabm.0c00335
ACS Appl. Bio Mater. 2020, 3, 4273−4281

Polymer Integrity Analysis in Living Materials. In certain applications, polymer integrity could be of essence in the LMs, but in other instances, a controlled polymer degradation might be preferred, making the study of polymer degradation an important component for development of LM-based technologies. F127-BUM contains carbamate bonds on the periphery of micelles, making it susceptible to enzymatic degradation by cells, which can secrete proteases,[32] and thus provides an excellent model for studying polymer degradation (Figures 1 and 6). To validate this idea, we conducted a 14 days experiment with and without a protease inhibitor cocktail for all of the LMs in the study (Figure 6). The concentration of inhibitors used in these experiments did not have an influence on control structures or on the cell proliferation. We used the fast release of gas in the supercritical CO_2 extraction protocol to identify differences between degraded and intact polymers in LMs (Figures 6 and S3.2).

The addition of inhibitors, as expected, did not have any effect on the outcome with F127-DMA and PGE-DMA compared to the control condition, as shown by similar images (Figure 6A,B,E,F). It should also be noted that in the case of PGE-DMA, the effect of the fast gas release appeared less pronounced compared to F127-based materials. This result could be attributed to the lower polymer concentration used in the formation of PGE-DMA hydrogels. During fast CO_2 extraction, less dense (or degraded) materials allow the gas to escape more easily (Figure 6C,E,F), whereas denser materials withhold the gas, resulting in cavities (Figure 6A,B,D). A clear difference was observed in the F127-BUM samples, where the sample appeared altered in the absence of the inhibitor, indicating a polymer degradation (Figure 6C,D). To ensure the reproducibility of these observations, we repeated the experiment for F127-BUM with a culture medium change every 48 h allowing secreted proteases more reaction time to potentially cleave the bonds. Following this approach, we found an even more pronounced difference, indicating a possible effect of enzymes on the integrity of F127-BUM (Figure S3.2E,F). The network degradation served as a reason for a lower cell retention time in F127-BUM compared with F127-DMA (Figure S2E), despite a higher storage modulus of the first. By simply changing the gas release speed, we could highlight how material properties change over time due to the confinement of cells. Using different proteases to study the enzyme degradation of F127-BUM might be worth an investigation in the future and can potentially make it an attractive candidate for use in biomedical applications, such as angiogenesis research, where enzyme-driven matrix degradation is vital.[33]

CONCLUSIONS

Our ability to develop new polymeric materials and their hydrogels for 3D printing LMs is outpacing our understanding of LMs due to the lack of investigations into how the mutual interactions of incorporated cells in the living materials impact both the cells and the polymers. Understanding such cellular−polymeric interactions is crucial to draw conclusions about the effects of physical confinement on cells within these materials.

We investigated three yeast-laden triblock copolymer hydrogel compositions (F127-DMA, F127-BUM, PGE-DMA) and characterized the condition of the encapsulated yeast colonies using scanning electron and optical microscopy techniques. These triblock copolymers self-assemble to form micelles or reverse micelles that afford shear-thinning hydrogel inks. The viscoelastic properties of the hydrogel were dependent upon both the polymer composition and the concentration in aqueous media and appear to affect the proliferation patterns of encapsulated yeast colonies and alteration of cell sizes. Of the polymers investigated, the F127-DMA hydrogels retained the cells the longest. When working with LMs, both physicochemical properties of the hydrogel and properties of immobilized cells have to be considered to analyze the interplay of cells and materials. Factors, such as the printing thickness and diffusion, should also be considered to ensure a sufficient nutrient supply to all cells within the LMs. Here, we have demonstrated changes in cellular phenotypes due to physical confinement within three hydrogels. However, our current study precludes an understanding of the underlying molecular mechanisms of phenotypic changes, which constitutes an important area of exploration that is currently underway.

ASSOCIATED CONTENT

Supporting Information

The Supporting Information is available free of charge at https://pubs.acs.org/doi/10.1021/acsabm.0c00335.

FTIR data for the three polymers; SEM micrographs; OM micrographs; measurements of the MM for different conditions; mass and cell retention time of LMs; LM photograph (PDF)

AUTHOR INFORMATION

Corresponding Authors

Rahul Kumar − *Institute of Technology, University of Tartu, 50411 Tartu, Estonia;* orcid.org/0000-0002-2277-9831; Email: rahul.kumar@ut.ee

Petri-Jaan Lahtvee − *Institute of Technology, University of Tartu, 50411 Tartu, Estonia*; Email: petri.lahtvee@ut.ee

Authors

Hans Priks − *Institute of Technology, University of Tartu, 50411 Tartu, Estonia*

Tobias Butelmann − *Institute of Technology, University of Tartu, 50411 Tartu, Estonia*

Aleksandr Illarionov − *Institute of Technology, University of Tartu, 50411 Tartu, Estonia*

Trevor G. Johnston − *Department of Chemistry, University of Washington, Seattle, Washington 98195, United States*

Christopher Fellin − *Department of Chemistry, University of Washington, Seattle, Washington 98195, United States*

Tarmo Tamm − *Institute of Technology, University of Tartu, 50411 Tartu, Estonia*

Alshakim Nelson − *Department of Chemistry, University of Washington, Seattle, Washington 98195, United States;* orcid.org/0000-0001-8060-8611

Complete contact information is available at: https://pubs.acs.org/10.1021/acsabm.0c00335

Author Contributions

[§]H.P. and T.B. contributed equally to this work.

Notes

The authors declare no competing financial interest.

ACKNOWLEDGMENTS

This project received funding from the European Union's Horizon 2020 research and innovation program under grant

agreement no. 668997 and the Estonian Research Council (grant PUT1488P). T.B. and H.P. would additionally like to acknowledge mobility grants MB-2018-1/25 by Bayerisches Hochschulzentrum für Mittel-, Ost- und Südosteuropa (BAYHOST) and the European Regional Development Fund, respectively. A.N. acknowledges the National Science Foundation (Grant No. 1752972), UW CoMotion Innovation Grant, and UW Royalty Research Fund for financial support of this work. We thank Külli Jaako and Monika Jürgenson, at the Institute of Biomedicine and Translational Medicine, Faculty of Medicine, University of Tartu, for access to their facility.

REFERENCES

(1) Dasgupta, Q.; Black, L. D. A Fresh Slate for 3D Bioprinting. *Science* **2019**, 446−447.
(2) Smith, P. T.; Basu, A.; Saha, A.; Nelson, A. Chemical Modification and Printability of Shear-Thinning Hydrogel Inks for Direct-Write 3D Printing. *Polymer* **2018**, *152*, 42−50.
(3) Huang, J.; Liu, S.; Zhang, C.; Wang, X.; Pu, J.; Ba, F.; Xue, S.; Ye, H.; Zhao, T.; Li, K.; Wang, Y.; Zhang, J.; Wang, L.; Fan, C.; Lu, T. K.; Zhong, C. Programmable and Printable Bacillus Subtilis Biofilms as Engineered Living Materials. *Nat. Chem. Biol.* **2019**, *15*, 34−41.
(4) Saha, A.; Johnston, T. G.; Shafranek, R. T.; Goodman, C. J.; Zalatan, J. G.; Storti, D. W.; Ganter, M. A.; Nelson, A. Additive Manufacturing of Catalytically Active Living Materials. *ACS Appl. Mater. Interfaces* **2018**, *10*, 13373−13380.
(5) Li, J.; Mooney, D. J. Designing Hydrogels for Controlled Drug Delivery. *Nat. Rev. Mater.* **2016**, *1*, No. 16071.
(6) Zhu, J.; Marchant, R. E. Design Properties of Hydrogel Tissue-Engineering Scaffolds. *Expert Rev. Med. Devices 8*, 607 626. DOI: 10.1586/erd.11.27.
(7) Qian, F.; Zhu, C.; Knipe, J. M.; Ruelas, S.; Stolaroff, J. K.; DeOtte, J. R.; Duoss, E. B.; Spadaccini, C. M.; Henard, C. A.; Guarnieri, M. T.; Baker, S. E. Direct Writing of Tunable Living Inks for Bioprocess Intensification. *Nano Lett.* **2019**, *19*, 5829−5835.
(8) Gopinathan, J.; Noh, I. Recent Trends in Bioinks for 3D Printing. *Biomater. Res.* **2018**, *22*, No. 11.
(9) Hölzl, K.; Lin, S.; Tytgat, L.; Van Vlierberghe, S.; Gu, L.; Ovsianikov, A. Bioink Properties before, during and after 3D Bioprinting. *Biofabrication* **2016**, *8*, No. 032002.
(10) Wu, W.; DeConinck, A.; Lewis, J. A. Omnidirectional Printing of 3D Microvascular Networks. *Adv. Mater.* **2011**, *23*, H178−H183.
(11) Fellin, C. R.; Adelmund, S. M.; Karis, D. G.; Shafranek, R. T.; Ono, R. J.; Martin, C. G.; Johnston, T. G.; DeForest, C. A.; Nelson, A. Tunable Temperature- and Shear-Responsive Hydrogels Based on Poly(Alkyl Glycidyl Ether)s. *Polym. Int.* **2019**, *68*, 1238−1246.
(12) Adams, M. L.; Lavasanifar, A.; Kwon, G. S. Amphiphilic Block Copolymers for Drug Delivery. *J. Pharm. Sci.* **2003**, *92*, 1343−1355.
(13) Chu, B.; Liu, T.; Wu, C.; Zhou, Z.; Mark Nace, V. Structures and Properties of Block Copolymers in Solution. *Macromol. Symp.* **1997**, *118*, 221−227.
(14) Malda, J.; Visser, J.; Melchels, F. P.; Jüngst, T.; Hennink, W. E.; Dhert, W. J. A.; Groll, J.; Hutmacher, D. W. 25th Anniversary Article: Engineering Hydrogels for Biofabrication. *Adv. Mater.* **2013**, *25*, 5011−5028.
(15) Pereira, R. F.; Bártolo, P. J. 3D Bioprinting of Photo-crosslinkable Hydrogel Constructs. *J. Appl. Polym. Sci.* **2015**, *132*, No. 42458.
(16) Wang, Z.; Kumar, H.; Tian, Z.; Jin, X.; Holzman, J. F.; Menard, F.; Kim, K. Visible Light Photoinitiation of Cell-Adhesive Gelatin Methacryloyl Hydrogels for Stereolithography 3D Bioprinting. *ACS Appl. Mater. Interfaces* **2018**, *10*, 26859−26869.
(17) Johnston, T. G.; Yuan, S.-F.; Wagner, J. M.; Yi, X.; Saha, A.; Smith, P.; Nelson, A.; Alper, H. S. Compartmentalized Microbes and Co-Cultures in Hydrogels for on-Demand Bioproduction and Preservation. *Nat. Commun.* **2020**, *11*, No. 563.
(18) Johnston, T. G.; Fellin, C. R.; Carignano, A.; Nelson, A. Poly(Alkyl Glycidyl Ether) Hydrogels for Harnessing the Bioactivity of Engineered Microbes. *Faraday Discuss.* **2019**, *219*, 58−72.
(19) Millik, S. C.; Dostie, A. M.; Karis, D. G.; Smith, P. T.; McKenna, M.; Chan, N.; Curtis, C. D.; Nance, E.; Theberge, A. B.; Nelson, A. 3D Printed Coaxial Nozzles for the Extrusion of Hydrogel Tubes toward Modeling Vascular Endothelium. *Biofabrication* **2019**, *11*, No. 045009.
(20) Drira, Z.; Yadavalli, V. K. Nanomechanical Measurements of Polyethylene Glycol Hydrogels Using Atomic Force Microscopy. *J. Mech. Behav. Biomed. Mater.* **2013**, *18*, 20−28.
(21) Shachaf, Y.; Gonen-Wadmany, M.; Seliktar, D. The Biocompatibility of PluronicF127 Fibrinogen-Based Hydrogels. *Biomaterials* **2010**, *31*, 2836−2847.
(22) Iurciuc Tincu, C.-E.; Savin, A.; Atanase, L. I.; Martin, P.; Popa, M. Physico-Chemical Characteristics and Fermentative Activity of the Hydrogel Particles Based on Polysaccharides Mixture with Yeast Cells Immobilized, Obtained by Ionotropic Gelation. *Food Bioprod. Process.* **2017**, *104*, 104−123.
(23) Iurciuc Tincu, C.-E.; Savin, A.; Atanase, L. I.; Danu, M.; Martin, P.; Popa, M. Encapsulation of *Saccharomyces cerevisiae* in Hydrogel Particles Based Gellan Ionically Cross-Linked with Zinc Acetate. *Powder Technol.* **2018**, *325*, 476−489.
(24) Bryant, S. J.; Cuy, J. L.; Hauch, K. D.; Ratner, B. D. Photo-Patterning of Porous Hydrogels for Tissue Engineering. *Biomaterials* **2007**, *28*, 2978−2986.
(25) Kim, S.-H.; Chu, C.-C. Synthesis and Characterization of Dextran-Methacrylate Hydrogels and Structural Study by SEM. *J. Biomed. Mater. Res.* **2000**, *49*, 517−527.
(26) Kim, S.-h.; Chu, C.-C. Pore Structure Analysis of Swollen Dextran-Methacrylate Hydrogels by SEM and Mercury Intrusion Porosimetry. *J. Biomed. Mater. Res.* **2000**, *53*, 258−266.
(27) U.S. Food & Drug Administration (FDA). *Code of Federal Regulations Title 21*; US Federal Government: Washington, 2019.
(28) Jiang, J.; Li, C.; Lombardi, J.; Colby, R. H.; Rigas, B.; Rafailovich, M. H.; Sokolov, J. C. The Effect of Physiologically Relevant Additives on the Rheological Properties of Concentrated Pluronic Copolymer Gels. *Polymer* **2008**, *49*, 3561−3567.
(29) Figueiredo, L.; Pace, R.; D'Arros, C.; Réthoré, G.; Guicheux, J.; Le Visage, C.; Weiss, P. Assessing Glucose and Oxygen Diffusion in Hydrogels for the Rational Design of 3D Stem Cell Scaffolds in Regenerative Medicine. *J. Tissue Eng. Regener. Med.* **2018**, *12*, 1238−1246.
(30) Sandrin, D.; Wagner, D.; Sitta, C. E.; Thoma, R.; Felekyan, S.; Hermes, H. E.; Janiak, C.; de Sousa Amadeu, N.; Kühnemuth, R.; Löwen, H.; Egelhaaf, S. U.; Seidel, C. A. M. Diffusion of Macromolecules in a Polymer Hydrogel: From Microscopic to Macroscopic Scales. *Phys. Chem. Chem. Phys.* **2016**, *18*, 12860−12876.
(31) Nagarajan, S.; Kruckeberg, A. L.; Schmidt, K. H.; Kroll, E.; Hamilton, M.; McInnerney, K.; Summers, R.; Taylor, T.; Rosenzweig, F. Uncoupling Reproduction from Metabolism Extends Chronological Lifespan in Yeast. *Proc. Natl. Acad. Sci. U.S.A.* **2014**, *111*, E1538−E1547.
(32) Moreno-García, J.; García-Martínez, T.; Mauricio, J. C.; Moreno, J. Yeast Immobilization Systems for Alcoholic Wine Fermentations: Actual Trends and Future Perspectives. *Front. Microbiol.* **2018**, *9*, No. 241.
(33) Song, K. H.; Highley, C. B.; Rouff, A.; Burdick, J. A. Complex 3D-Printed Microchannels within Cell-Degradable Hydrogels. *Adv. Funct. Mater.* **2018**, *28*, No. 1801331.

https://dx.doi.org/10.1021/acsabm.0c00335
ACS Appl. Bio Mater. 2020, 3, 4273−4281